2011 50th IEEE Conference on Decision and Control and
European Control Conference (CDC-ECC)
Orlando, FL, USA, December 12-15, 2011

Control of a multi-axis platform for metrological purposes using differential flatness

J.M.Rodriguez-Fortun, J.Orus, J.Alfonso, F.Rotella, J.A.Castellanos

Abstract— **Positioning and tracking devices with micrometer range and sub-micrometer resolution are becoming of special interest in recent years for an extending range of applications including metrological devices, manipulators and mechanization systems both in research and high precision industries (for example, semiconductors). The control of these systems is not an easy task because of its normally high stiffness and the coupling existing between the different degrees of freedom. The present work proposes a control strategy based on differential flatness for static positioning and dynamic trajectory tracking with a platform of three degrees of freedom. The system uses piezoelectric actuators and is specially conceived for metrological devices, which do not suffer important external loads. The proposed method permits to decouple the design of a closed loop control for each degree of freedom and calculates an open loop command directly from the trajectory definition in the three degrees of freedom. The performance of the controller has been experimentally checked both in positioning and tracking applications.**

I. INTRODUCTION

The present work describes a control strategy for positioning and trajectory tracking with micrometer range and sub-micrometer resolution of a platform with three degrees of freedom: vertical movement (z), tip (θ_x) and tilt (θ_y). The system is specially developed for metrological systems, like Atomic Force Microscopes (AFM), with no external loads applied to the platform.

Platforms for high precision positioning and tracking constitute an important field of research and development. These devices can be used in metrological systems, like the one described in this work, but its range of application extends to many other fields, like micromechanics, micromechanization and micro-biology [4], among others. For applications requiring larger ranges of movement, the so called manipulator systems are used [12]. These systems combine a first stage using large range actuators with a second stage using micrometer range actuators for increasing the resolution of the former. There is a number of different devices depending on the final purpose or the number of degrees of freedom. Using these last characteristic as reference, literature describes examples with: one degree of freedom, like the single-axis displacement systems described in [5] and [6]; two degrees of freedom, like the XY positioning system in [10]; three degrees of freedom, like the RRR-platform in [4] or the $XY\theta$ platform in [9]; and with six degrees of freedom, like [11]. The device used in present work uses a tripod structure with three actuation lines which adapt the concept described in [7] by increasing stiffness and robustness according to its final purpose. This structure presents important benefits with respect to typical tripod positioners because of its low thickness structure and high stiffness in x, y directions (horizontal displacements).

Two elements are of major importance in the design of high precision positioning and tracking systems: joints and actuators. In the first case, joints between elements are mostly flexures, also named compliant links [18] based on deformable elements which have a much lower stiffness in the direction of interest compared with the others. These elements avoid friction between parts, reduce backlash effects and have a linear behaviour in the displacement range. With respect to the actuators, they must be accurate and permit a high movement resolution. In this connection, piezoelectric actuators fit perfectly to this purpose and can be found in many of the systems previously mentioned like [7][4][5]. However, there are designs based on other actuator types, like DC linear motors [15], electrostatic actuators [16], Shape Memory Alloys [12], among others. The platform object of the present work uses amplified piezoelectric actuators because of its compactness, response time and robustness.

With respect to the control methods, it is possible to find many different approaches depending on the particularities of the system: kinematics, actuators or final purpose. Examples of these methods are: PID compensators, robust μ-synthesis [14], backstepping [17], robust impedance control [8], among others. For the platform design used in the present work, a global control strategy based on differential flatness is proposed [1][2][3]. Compared to other approaches, the proposed controller permits directly obtaining the command to the three actuators from the description of the platform movement in the global coordinates (z, θ_x, θ_y) and controlling the error in the three degrees of freedom in a decoupled way, which highly simplifies the design process.

The details of the present work are described in next sections. Section II describes the platform. Section III presents the mathematical model of the device, which will be subsequently used for defining the control strategy in section IV. The results of the implementation are described in section

J.M.Rodriguez-Fortun, J.Orus and J.Alfonso are with the Grupo de Investigación Aplicada (GIA-MDPI), Instituto Tecnológico de Aragón, Zaragoza, Spain (e-mail:{jmrodriguez, jorus, jalfonso}@ita.es).

F.Rotella is with ENIT, Tarbes, France (e-mail:rotella@enit.fr).

J.A.Castellanos is with the Instituto de Ingeniería de Aragón, Universidad de Zaragoza, Spain (e-mail:jacaste@unizar.es).

This work is part of RICAT+ project, supported by FEDER funds (Programa Operativo de Cooperación Territorial España-Francia-Andorra 2007-2013). Activities in collaboration with I3A partially funded by HYPER project (Consolider-Ingenio 2010).

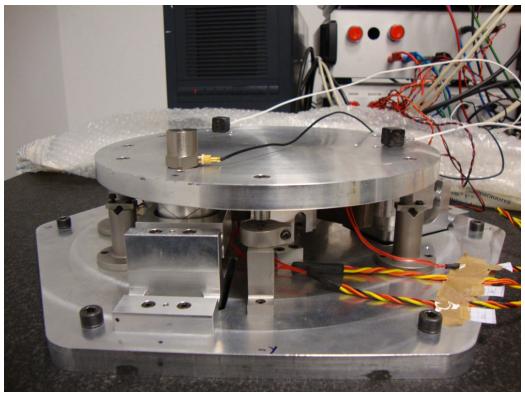

Fig. 1. Picture of the platform. In the image the three accelerometers at the upper part of the actuation line can be observed. Additionally, three strain gauges are embedded in the piezoelectric actuators.

V.

II. DESCRIPTION OF THE PLATFORM

The platform object of the present work appears in figure 1 and it is intended for arranging accurate displacements in three degrees of freedom: z, θ_x and θ_y (axis can be observed in figure 5).

The system is based on a tripod structure with three actuation lines shifted 120 degrees. Figure 2 shows the structure of one actuation line and its relative position. This morphology is described in [7] and places the actuator between two flexures of one degree of freedom. The actuator moves parallel to the xy plane. The actuation direction is modified from horizontal to vertical direction by using a lever. The restrictions created by the flexures define a preferred direction of movement, presenting an increased stiffness in the other directions. Finally, the vertical movement is transmitted to the upper platform by means of a vertical link between platform and lever. The design of the flexures varies from [7] and flexures with one degree of freedom are preferred over the original links with multiple degrees of freedom. This condition is only relaxed for the connection between the upper platform and the vertical link, which uses hinges with two-degrees of freedom for the rotation in axes x and y. This configuration increases the stiffness of the system in all directions.

The piezoelectric actuator APA-120ML from Cedrat Group is used. This actuator uses a cymbal for amplifying the stroke and it is characterized by a high robustness to tangent forces, which is of great importance when mounting it in a structure with geometrical tolerances between parts.

III. MATHEMATICAL MODEL OF THE PLATFORM

The next description outlines the mathematical derivation of a state space representation for the platform. The details of the derivation can be found in the technical report [20]. This model is characterized by:

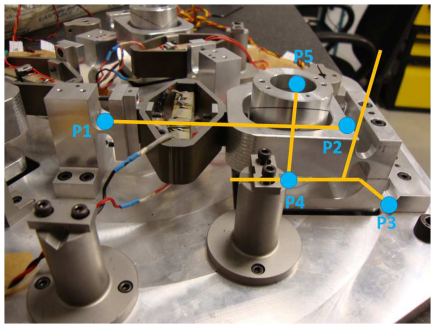

Fig. 2. Image of an actuation line. A kinematic model is overimposed in yellow, with the joints represented as blue spheres.

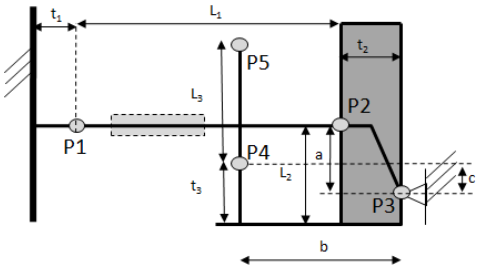

Fig. 3. Main elements and dimensions of an actuation line.

- States: position ($\mathbf{x}$), velocity ($\dot{\mathbf{x}}$) of the upper platform in the three degrees of freedom and charge ($\mathbf{q}$) in the three piezoelectric actuators (figure 5):

$$\mathbf{x} = \begin{pmatrix} z \\ \theta_x \\ \theta_y \end{pmatrix}, \dot{\mathbf{x}} = \begin{pmatrix} \dot{z} \\ \dot{\theta}_x \\ \dot{\theta}_y \end{pmatrix}, \mathbf{q} = \begin{pmatrix} q_a \\ q_b \\ q_c \end{pmatrix} \quad (1)$$

- System inputs: the input voltage to the three actuators a, b and c:

$$\mathbf{v} = \begin{pmatrix} V_a \\ V_b \\ V_c \end{pmatrix} \quad (2)$$

In the application of interest, the external forces can be neglected.

This representation is sequentially obtained by defining the behaviour of each single actuation line and finally coupling them using the rotation of the upper platform and the dynamic loads. Figures 3 and 4 show a simple representation of an actuation line and its main dimensions:

- Assuming small displacements of the actuator j (δ_j), the angles α_i of each joint P_i are (figure 4):

$$\begin{aligned} \alpha_1 &\approx 0 \\ \alpha_2 &= \alpha_1 + \alpha_3 \approx \alpha_3 \\ \alpha_3 &\approx \frac{\delta_j}{t_4 \sin(\pi/2-\beta)} \\ \alpha_4 &\approx \alpha_3 \\ \alpha_5 &\approx 0 \end{aligned} \quad (3)$$

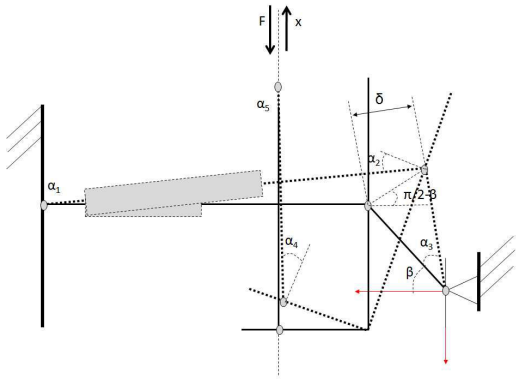

Fig. 4. Angles of one actuation line when the piezoelectric actuator changes its length. For clarity reasons, subindexes j for the three lines have not been included in F and x.

With $t_4 = \sqrt{t_2^2 + a^2}$.

- The relation between $\delta_{p,j}$, the deformation at a definite voltage if no load is applied on the actuator j, and the displacement (x_j) in figure 4 is obtained as:

$$x_j = A_1 \delta_{p,j} - A_2 F_j \tag{4}$$

Where,

$$\begin{array}{rcl} A_1 & = & \frac{k_{e1} a_m b}{k_{e1} a a_m + (k_{b2}+k_{b3}+k_{b4})} \\ A_2 & = & \left(\frac{1}{k_{e3}} + \frac{a_m b^2}{k_{e1} a^2 a_m + (k_{b2}+k_{b3}+k_{b4})} \right) \\ a_m & = & t_4 \sin\left(\pi/2 - \beta\right) \\ \delta_{p,j} & = & a_{pzt} q_j \\ k_{e1} & = & \left(\frac{1}{k_{a1}} + \frac{1}{k_{a2}} + \frac{1}{k_p} \right)^{-1} \\ k_{e3} & = & \left(\frac{1}{k_{a4}} + \frac{1}{k_{a5}} \right)^{-1} \end{array} \tag{5}$$

In expressions above, k_{e1} is the equivalent stiffness in the horizontal bar, and k_{e3} is the stiffness of the pillar. k_{ai} and k_{bi} represent the axial and rotation stiffness of joint i. k_p and a_{pzt} are the stiffness and the electromechanical transformation factor of the actuator.

- The force applied at the actuator j ($F_{1,j}$) because of the displacement x_j and the load F_j is:

$$F_{1,j} = B_1 F_j + B_2 x_j \tag{6}$$

Where,

$$\begin{array}{rcl} B_1 & = & \frac{b}{a} + \frac{1}{b k_{e3} a_m} \left(k_{b2} + k_{b3} + k_{b4} \right) \\ B_2 & = & \frac{1}{b a_m} \left(k_{b2} + k_{b3} + k_{b4} \right) \end{array} \tag{7}$$

The coupling between the three actuation lines is obtained by:

- The relative transformation between the degrees of freedom of the platform and the vertical movement of the three actuation lines (a, b, c) linked to the former at a distance r from its center (figure 5):

$$\mathbf{f} = \mathbf{T}_f \mathbf{f}_{abc}, \; \mathbf{x} = \left(\mathbf{T}_f^T \right)^{-1} \mathbf{x}_{abc} \tag{8}$$

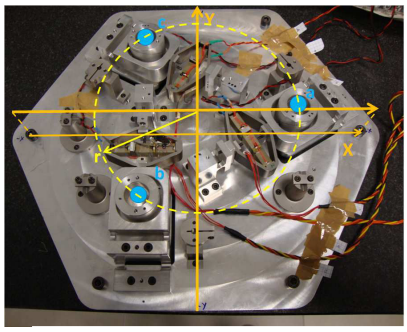

Fig. 5. Image of the platform with a representation of the reference axis in yellow and the nomenclature adopted for the three actuation lines (a, b and c). The actuation lines are shifted 120 degrees.

Where,

$$\begin{array}{rcl} \mathbf{T}_f & = & \begin{pmatrix} 1 & 1 & 1 \\ 0 & -r\cos(\pi/6) & r\cos(\pi/6) \\ -r & r\sin(\pi/6) & r\sin(\pi/6) \end{pmatrix} \\ \mathbf{f} & = & \begin{pmatrix} F_z \\ \Gamma_x \\ \Gamma_y \end{pmatrix} \\ \mathbf{f}_{abc} & = & \begin{pmatrix} F_a \\ F_b \\ F_c \end{pmatrix} \end{array} \tag{9}$$

In previous expressions, subindexes a, b and c refer to local values of the actuation lines. F_k and Γ_k stand for forces and torques in direction k ($k = x, y, z$).

- The coupling effect of the upper platform by the dynamic loads and the rotation angles θ_x and θ_y:

$$\mathbf{f} = \mathbf{M}\ddot{\mathbf{x}} + \mathbf{C}_v \dot{\mathbf{x}} + \mathbf{D}\mathbf{x} \tag{10}$$

With,

$$\begin{array}{rcl} \mathbf{M} & = & \begin{pmatrix} M & 0 & 0 \\ 0 & J_x & 0 \\ 0 & 0 & J_y \end{pmatrix} \\ \mathbf{D} & = & \begin{pmatrix} 0 & \mathbf{0}_{1\times 2} \\ \mathbf{0}_{2\times 1} & -\mathbf{T}_{\alpha 5}^T \mathbf{K}_{\alpha 5} \mathbf{T}_{\alpha 5} \end{pmatrix} \\ \mathbf{T}_{\alpha 5} & = & \begin{pmatrix} \cos(\pi/3) & \cos(\pi/6) \\ -\sin(\pi/3) & \sin(\pi/6) \\ \cos(\pi/3) & -\cos(\pi/6) \\ \sin(\pi/3) & \sin(\pi/6) \\ -1 & 0 \\ 0 & -1 \end{pmatrix} \\ \mathbf{K}_{\alpha 5} & = & \begin{pmatrix} \mathbf{k}_{b5} & \mathbf{0} & \mathbf{0} \\ \mathbf{0} & \mathbf{k}_{b5} & \mathbf{0} \\ \mathbf{0} & \mathbf{0} & \mathbf{k}_{b5} \end{pmatrix} \\ \mathbf{k}_{b5} & = & \begin{pmatrix} k_{b5,x} & k_{b5,xy} \\ k_{b5,xy} & k_{b5,y} \end{pmatrix} \end{array} \tag{11}$$

$\mathbf{M}$ stands for an inertia matrix in the three degrees of freedom, $\mathbf{C}_v$ is a viscous friction term, and $\mathbf{D}$ is the stiffness associated with the line 5.

$\delta_{p,j}$ can be related with the electrical charge q_j in the actuator j (5) which depends on the input voltage by [19]:

$$\dot{q}_j = \frac{1}{R_e}\left(V_j - \frac{q_j}{C} + a_{pzt}F_{1,j}\right) \tag{12}$$

where,

V_j : voltage applied to the actuator j $[V]$
q_j : charge in the piezoelectric capacitor j $[C]$
R_e : electric resistance from amplifier to actuator $[\Omega]$
C : capacitance value of the actuator $[F]$

Combining (4), (6), (10) and (12) the state space representation results:

$$\begin{aligned}\begin{pmatrix}\dot{\mathbf{x}}\\ \ddot{\mathbf{x}}\\ \dot{\mathbf{q}}\end{pmatrix} &= \begin{pmatrix}\mathbf{0}_{3\times3} & \mathbf{1}_{3\times3} & \mathbf{0}_{3\times3}\\ -\mathbf{H}_1 & -\mathbf{H}_2 & -\mathbf{H}_3\\ \mathbf{H}_4 & \mathbf{H}_5 & \mathbf{H}_6\end{pmatrix}\begin{pmatrix}\mathbf{x}\\ \dot{\mathbf{x}}\\ \mathbf{q}\end{pmatrix} + \\ &\quad \begin{pmatrix}\mathbf{0}_{3\times3}\\ \mathbf{0}_{3\times3}\\ \mathbf{H}_7\end{pmatrix}\mathbf{v} \\ &= \mathbf{A}_{ss}\mathbf{x}_{ss} + \mathbf{B}_{ss}\mathbf{v}\end{aligned} \tag{13}$$

With,

$$\begin{aligned}\mathbf{H}_0 &= \mathbf{a}_{pzt}\mathbf{B}_1\mathbf{T}_f^{-1}\\ \mathbf{H}_1 &= \left(\mathbf{A}_2\mathbf{T}_f^{-1}\mathbf{M}\right)^{-1}\left(\mathbf{T}_f^T + \mathbf{A}_2\mathbf{T}_f^{-1}\mathbf{D}\right)\\ \mathbf{H}_2 &= \left(\mathbf{A}_2\mathbf{T}_f^{-1}\mathbf{M}\right)^{-1}\mathbf{A}_2\mathbf{T}_f^{-1}\mathbf{C}_v\\ \mathbf{H}_3 &= \left(\mathbf{A}_2\mathbf{T}_f^{-1}\mathbf{M}\right)^{-1}\mathbf{A}_1\mathbf{a}_{pzt}\\ \mathbf{H}_4 &= \mathbf{R}_e^{-1}\left(\mathbf{a}_{pzt}\mathbf{B}_2\mathbf{T}_f^T + \mathbf{H}_0\mathbf{D} - \mathbf{H}_0\mathbf{M}\mathbf{H}_1\right)\\ \mathbf{H}_5 &= \mathbf{R}_e^{-1}\left(\mathbf{H}_0\mathbf{C}_v - \mathbf{H}_0\mathbf{M}\mathbf{H}_2\right)\\ \mathbf{H}_6 &= \mathbf{R}_e^{-1}\left(-\mathbf{C}^{-1} - \mathbf{H}_0\mathbf{M}\mathbf{H}_3\right)\\ \mathbf{H}_7 &= \mathbf{R}_e^{-1}\end{aligned} \tag{14}$$

$\mathbf{A}_1$, $\mathbf{A}_2$, $\mathbf{B}_1$, $\mathbf{B}_2$, $\mathbf{R}_e$, $\mathbf{C}$ and $\mathbf{a}_{pzt}$ are diagonal matrices with the terms in the diagonal equal to the scalar value of the same name.

System (13) is controllable, as it can be easily checked by calculating the rank of the controllability matrix $\mathbf{C}_{ss}$:

$$\mathbf{C}_{ss} = \begin{pmatrix}\mathbf{B}_{ss} & \mathbf{A}_{ss}\mathbf{B}_{ss} & \mathbf{A}_{ss}^2\mathbf{B}_{ss}\end{pmatrix} \tag{15}$$

IV. CONTROL STRATEGY

The proposed controller uses differential flatness for its design. This property and its influence in the controller design is described in this section.

A. Differential flatness

Differential flatness is a property of a system which permits to express its states $\mathbf{x}$ and inputs $\mathbf{u}$ in terms of the so called *flat outputs* $\mathbf{y}$, which are equal in number to the inputs of the system, and a finite number of their derivatives [1]. This property has two important consequences:

- The input values $\mathbf{v}$ (2) are directly obtained from the definition of the desired trajectory in terms of the *flat outputs* and their derivatives.
- The system expressed in flat coordinates has a trivial shape.

By definition, a controllable linear system is flat [3] and therefore it can be expressed in terms of its *flat outputs*. In (13), the states $\mathbf{x}$ are the flat outputs $\mathbf{y}$ and the equivalence between the original and the flat representation can be expressed by means of the following diffeomorphism:

- In one direction:

$$\begin{aligned}\mathbf{x} &= \mathbf{y}\\ \dot{\mathbf{x}} &= \dot{\mathbf{y}}\\ \mathbf{q} &= \mathbf{H}_3^{-1}\left(-\ddot{\mathbf{y}} - \mathbf{H}_1\mathbf{y} - \mathbf{H}_2\dot{\mathbf{y}}\right)\end{aligned} \tag{16}$$

- In the other direction:

$$\begin{aligned}\mathbf{y} &= \mathbf{x}\\ \dot{\mathbf{y}} &= \dot{\mathbf{x}}\\ \ddot{\mathbf{y}} &= -\mathbf{H}_1\mathbf{x} - \mathbf{H}_2\dot{\mathbf{x}} - \mathbf{H}_3\mathbf{q}\end{aligned} \tag{17}$$

The transformed system (13) has the shape:

$$\dddot{\mathbf{y}} = \xi \tag{18}$$

With ξ the input of the system.

B. Design of the compensator

Once the transformation is defined, we focus on the design of the control strategy. To do that, the dynamics of the error $\mathbf{e}$ is expressed as:

$$\dddot{\mathbf{e}} = \dddot{\mathbf{y}}_{ref} - \dddot{\mathbf{y}} \tag{19}$$

Where $\mathbf{y}_{ref}$ is the reference trajectory.
Defining the input as:

$$\xi = \dddot{\mathbf{y}}_{ref} + \mathbf{w} \tag{20}$$

The error dynamics results in:

$$\dddot{\mathbf{e}} = -\mathbf{w} \tag{21}$$

As (21) is decoupled in z, θ_x and θ_y, the control strategy can be defined locally in each degree of freedom j as:

$$w_j = K_{fl,j}\ddot{e}_j \tag{22}$$

Including (22) in (20):

$$\begin{aligned}\dddot{\mathbf{y}} &= \xi = \dddot{\mathbf{y}}_{ref} + \mathbf{K}_{fl}\ddot{\mathbf{e}}\\ \ddot{\mathbf{y}} &= \ddot{\eta} = \ddot{\mathbf{y}}_{ref} + \mathbf{K}_{fl}\dot{\mathbf{e}}\\ \dot{\mathbf{y}} &= \dot{\eta} = \dot{\mathbf{y}}_{ref} + \mathbf{K}_{fl}\mathbf{e}\\ \mathbf{y} &= \eta = \mathbf{y}_{ref} + \mathbf{K}_{fl}\int\mathbf{e}dt\end{aligned} \tag{23}$$

With $\mathbf{K}_{fl}$ a diagonal matrix. As observed, the error behaves like a first order system.

The error signals are estimated from the sensor data available, avoiding integration steps that could result in windup problems. The sensors installed in the system are:

- Strain gauges embedded in the piezoelectric actuators: they measure the value δ_j in the actuators, which can be used for estimating $\mathbf{y}$ using (8) and the lever ratio.
- Accelerometers at the top of the three actuation lines: they are used for estimating $\ddot{\mathbf{y}}$ and, their integrated value, for estimating $\dot{\mathbf{y}}$. As before, the geometrical relationship (8) is used.

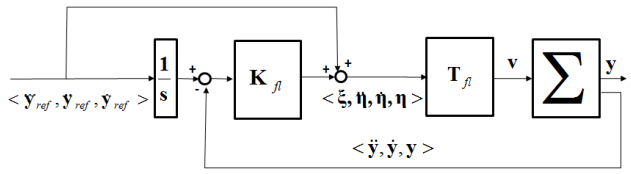

Fig. 6. Diagram of the control strategy showing: $\mathbf{K}_{fl}$, the closed loop compensator in the flat coordinates; $\mathbf{T}_{fl}$, equivalence between the flat states and the output voltage.

C. Voltage equivalence

The input voltage in the actuators is obtained using its equivalence with the *flat outputs* and their derivatives as:

$$\begin{aligned}\mathbf{v} \;=\; & \mathbf{T}_{fl}\left(\xi,\ddot{\eta},\dot{\eta},\eta\right) = -\mathbf{H}_7^{-1}\mathbf{H}_3^{-1}\xi + \\ & \left(-\mathbf{H}_7^{-1}\mathbf{H}_3^{-1}\mathbf{H}_2 + \mathbf{H}_7^{-1}\mathbf{H}_6\mathbf{H}_3^{-1}\right)\ddot{\eta} + \\ & \left(-\mathbf{H}_7^{-1}\mathbf{H}_3^{-1}\mathbf{H}_1 - \mathbf{H}_7^{-1}\mathbf{H}_5 + \mathbf{H}_7^{-1}\mathbf{H}_6\mathbf{H}_3^{-1}\mathbf{H}_2\right)\dot{\eta} \\ & + \left(-\mathbf{H}_7^{-1}\mathbf{H}_4 + \mathbf{H}_7^{-1}\mathbf{H}_6\mathbf{H}_3^{-1}\mathbf{H}_1\right)\eta\end{aligned} \tag{24}$$

V. EXPERIMENTAL RESULTS

The behaviour of the system has been experimentally checked in two different conditions:

- Positioning the upper platform in static conditions.
- Trajectory tracking in the three degrees of freedom.

A. Positioning experiment

Figure 7 shows the behaviour of the system when three stepped reference signals are commanded to the system at the same time. For assuring the continuity of the reference position, which is required for calculating the command (24), the steps are described by means of sharp slope sinusoids. As observed, reference and experimental lines coincide. The error can be observed in figure 8.

In stationary conditions, the maximum error is $\pm 18nm$ in z, $\pm 0.21\mu rad$ in θ_x and θ_y and is mainly caused by sensor noise. The error slightly increases between the transitions from one level to the next one during signal tracking. More details on tracking are given in next subsection.

B. Tracking experiment

The performance of the system in tracking conditions is evaluated using random signals. These signals are generated at $20kHz$, and filtered with a fourth order low-pass filter for reducing the high frequency content to the desired limit. These signals are differently generated for the three degrees of freedom.

Figure 9 shows the behaviour of the system when the reference trajectory is a random signal with its main frequency content below $5Hz$. As observed, reference and tracked signal perfectly match. The tracking error appears in figure 10. The *RMS* error with respect to the *RMS* value of the reference signal is: 0.4% in z, 0.6% in θ_x and 0.4% in θ_y. If the *RMS* error is referred to the maximum value of the reference signal, the relative error is: 0.11% in z, 0.29% in θ_x and 0.21% in θ_y.

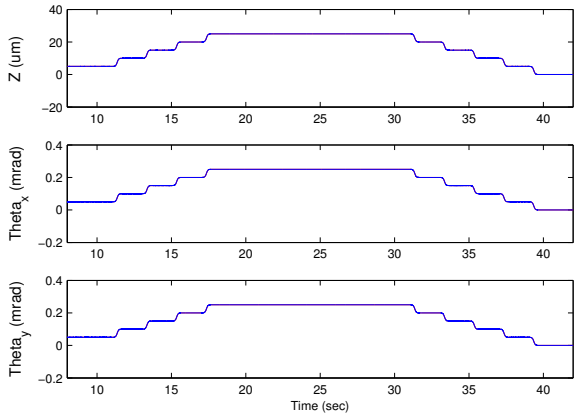

Fig. 7. Performance in positioning applications. In red, the reference signal, and in blue, the experimental value estimated from the strain gauges embedded in the actuators.

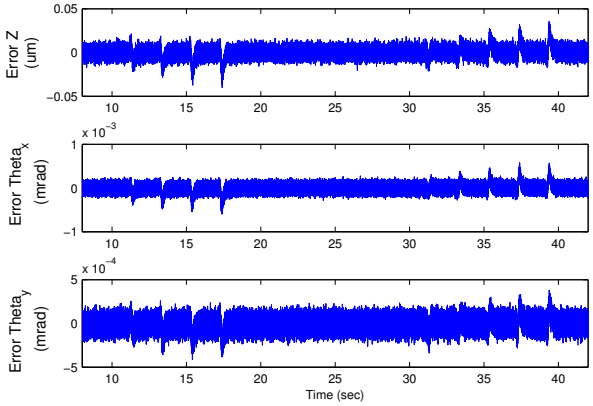

Fig. 8. Error signal during positioning.

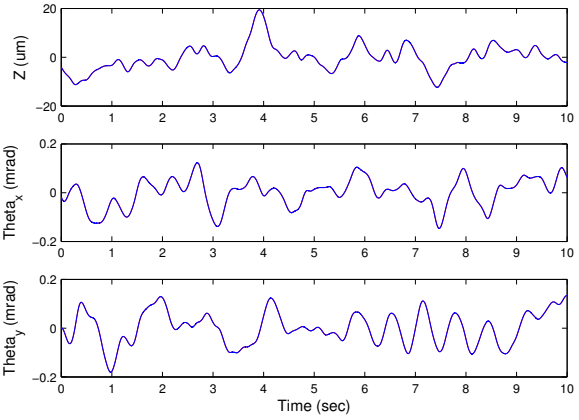

Fig. 9. Performance in tracking applications using reference signals with its main frequency content below $5Hz$. In red, the reference signal, and in blue, the experimental value estimated from the strain gauges embedded in the actuators.

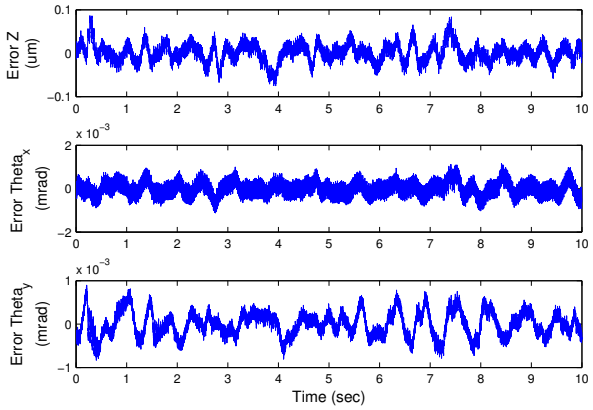

Fig. 10. Tracking error using a reference signal with its main frequency content below $5Hz$.

VI. CONCLUSIONS AND FUTURE WORK

The present work describes a control strategy based on differential flatness for a multi-axis positioning and trajectory tracking platform of micrometer range. The platform has three degrees of freedom: vertical displacement, tip and tilt. Once the differential flatness has been demonstrated by means of the system controllability, the position described in terms of the three global coordinates (z, θ_x, θ_y) is proved to be the *flat output* of the system and therefore, system behaviour can be completely described in terms of the reference trajectory and its derivatives. As a consequence, the control strategy permits: on the one hand, defining a feedforward command in open loop conditions directly from the trajectory definition; and on the other hand, designing a closed loop compensator in a decoupled way for each degree of freedom of the platform. Compared with other decoupled approaches based on the local control of the three actuators, the flatness-based controller proposed maintains the information about the coupling effects between the actuators.

The platform has been experimentally evaluated in positioning and tracking applications. In the first case, the obtained position estimate oscillates $\pm 18nm$ in z, $\pm 0.21\mu rad$ in θ_x and θ_y with respect to the reference signal. This oscillation is caused by the sensor noise. In the second case, platform has been tested with three different random reference signals applied at the same time in the three degrees of freedom. The result obtained using random signals with frequency components below $5Hz$ is: 0.4% in z, 0.6% in θ_x and 0.4% in θ_y. These values are described in terms of *RMS* errors with respect to the *RMS* value of the reference signal.

This work is part of a larger project for designing a three-axis platform which could be used for positioning, tracking or active vibration control, depending on the final application. The description above is centered on positioning and tracking applications, remaining vibration damping as a future activity. Current tasks are focused on the calibration of the system, increase of the tracking bandwidth, hysteresis compensation and evaluation of other estimation techniques for the flat states.

VII. ACKNOWLEDGMENTS

The authors acknowledge the collaboration of J.R.Sierra for his support during the experimental activities.

REFERENCES

[1] M.Fliess, J.Levine, Ph.Martin, P.Rouchon, "Sur les systèmes non linéaires différentiellement plats," Comptes Rendus de l'Académie des sciences Paris, I315 (1992). 619-624.

[2] M.Fliess, J.Levine, Ph.Martin, P.Rouchon, "Flatness and defect of nonlinear systems: introductory theory and examples," International Journal of Control, v.61:6 (1995). 1327-1361.

[3] J.Levine, "Analysis and control of nonlinear systems: a flatness-based approach," Springer, 2009.

[4] Y.K.Yong, T.-F.Lu, "Kinetostatic modeling of 3-RRR compliant micro-motion stages with flexure hinges," Mechanism and Machine Theory, v.44 (2009). 1156-1175.

[5] Y.Tian, B.Shirinzadeh, D.Zhang, "A flexure-based mechanism and control methodology for ultra-precision turning operation," Precision Engineering, v.33 (2009). 160-166.

[6] Y.Tian, B.Shirinzadeh, D.Zhang, G.Alici, "Development and dynamic modelling of a flexure-based ScottRussell mechanism for nano-manipulation," Mechanical Systems and Signal Processing, v.23(2009).957-978.

[7] H.S.Kim, Y.M.Cho, "Design and modeling of a novel 3-DOF precision micro-stage," Mechatronics, v.19:5 (2009). 598-608.

[8] H.C.Liaw, B.Shirinzadeh, "Robust generalised impedance control of piezo-actuated flexure-based four-bar mechanisms for micro/nano manipulation," Sensors and Actuators A, v.148 (2008). 443-453.

[9] D.Mukhopadhyay, J.Dong, E.Pengwang, P.Ferreira, "A SOI-MEMS-based 3-DOF planar parallel-kinematics nanopositioning stage," Sensors and Actuators A, v.147 (2008). 340-351.

[10] Y.-J.Choi, S.V.Sreenivasan, B.J.Choi, "Kinematic design of large displacement precision XY positioning stage by using cross strip flexure joints and over-constrained mechanism," Mechanism and Machine Theory, v.43 (2008). 724-737.

[11] J.E.McInroy, "Modeling and Design of Flexure Jointed Stewart Platforms for Control Purposes," IEEE/ASME Transactions on Mechatronics, v.7:1 (2002). 95-99.

[12] P.R.Ouyang, R.C.Tjiptoprodjo, W.J.Zhang, G.S.Yang, "Micro-motion devices technology: The state of arts review," The International Journal of Advanced Manufacturing Technology, v.35:5-6 (2007). 463-478.

[13] Y.Chen, J.E.McInroy, "Decoupled Control of Flexure-Jointed Hexapods Using Estimated Joint-Space Mass-Inertia Matrix," IEEE Transactions on Control Systems Technology, v.12:3 (2004). 413-421.

[14] H.S.Kim, Y.M.Cho, J.H.Moon, "Active vibration control using a novel three-DOF precision micro-stage,"Smart Materials and Structures, v.19 (2010).

[15] S.Q.Lee, Y.Kim, D.-G.Gweon, "Continuous gain scheduling control for a micro-positioning system:simple, robust and no overshoot response," Control Engineering Practice, v.8 (2000). 133-138.

[16] M.Vagia, G.Nikolakopoulos, A.Tzes, "Design of a robust PID-control switching scheme for an electrostatic microactuator," Control Engineering Practice, v.16 (2008). 1321- 1328.

[17] H.-J.Shieh, F.-J.Lin, P.-K.Huang, L.-T.Teng, "Adaptive tracking control solely using displacement feedback for a piezo-positioning mechanism," IEE Proceedings on Control Theory and Applications, v.151:5 (2004). 653-660.

[18] S.T.Smith, "Flexures: Elements of Elastic Mechanisms," Gordon & Breach Science Pub (2000).

[19] J.M.Rodriguez-Fortun, J.Orus, F.Buil, J.A.Castellanos, "General Bond Graph model for piezoelectric actuators and methodology for experimental identification," Mechatronics, v.20:2 (2010). 303-314.

[20] J.M.Rodriguez-Fortun, "Mathematical derivation of a state representation for a three axis micropositioning platfom," Technical report 2400I119008 (http://kristal-priv.ita.es/ricat/images/documents/2400I119008.pdf).